JOURNAL OF CATALYSIS 123, 285–297 (1990)

Metal–Support Interaction in the Pd/SiO_2 System: Influence of the Support Pretreatment[1]

RYSZARD LAMBER,* NILS JAEGER,† AND GÜNTER SCHULZ-EKLOFF†

*Institute of Low Temperature and Structure Research, Polish Academy of Sciences, 50-950 Wrocław, P.O. Box 937, Poland; and †Institut für Angewandte und Physikalische Chemie, Universität Bremen, D-2800 Bremen 33, Federal Republic of Germany

Received December 1, 1987; revised May 4, 1989

Transmission electron microscopy, electron diffraction, and convergent beam diffraction have been used to study strong metal–support interaction in the Pd/SiO_2 system. It has been shown that heating of the palladium/silica system in a hydrogen atmosphere may lead to chemical (strong) interaction between metal and support and growth of palladium silicide (Pd_2Si). Microdiffraction analysis shows an oriented growth of the Pd_2Si precipitate with respect to the Pd matrix. The magnitude of metal–support interaction, the agglomeration of metal particles, and the formation of an intermetallic compound are strongly influenced by the thermal pretreatment of the SiO_2 substrate. The presence of silanol groups (SiOH) on the silica surface seems to facilitate the metal particle migration and growth by coalescence, in contrast to OH-depleted silica where the change in the particle size proceeds by atomic diffusion. The presence of silanol groups may facilitate chemical metal–support interaction and formation of an intermetallic compound.

INTRODUCTION

Silica, one of the most frequently used supports in heterogeneous catalysis, is usually considered to be an inert substrate for metal particles, although some results of the investigations of noble metals supported on SiO_2 have demonstrated that temperature and the nature of the gas atmosphere may seriously influence the interaction of deposited metals with this support. The strong chemical interaction can be observed as changes in the adsorptive and catalytic properties of the catalysts and/or a formation of an intermetallic compound. Wilson and Hall (*1*) observed the apparent decrease in H_2 chemisorption after treatment of Pt/SiO_2 in H_2 at 1040 K with no accompanying change in average Pt particle size. For the Pd/SiO_2 system, Moss *et al.* (*2*) established that raising the reduction temperature to 873 K caused formation of a palladium–silicon intermetallic compound. They assumed that some interaction of palladium and silicon occurred at temperatures below 873 K and could be responsible for the decrease in the specific activity for benzene hydrogenation. Martin *et al.* (*3–5*) reported that raising the temperature of the reduction of Ni/SiO_2 and Pt/SiO_2 to 1120 K results in a decrease in catalytic activity in hydrogenation and hydrogenolysis. This behavior is believed to be connected with the formation of a metal silicide, which was confirmed for the Ni/SiO_2 system by magnetic measurements (*6*). During examination of the purity of the surfaces of platinum films evaporated on quartz, van Langeveld *et al.* (*7*) established that the surface of the platinum films is contaminated by silicon and concluded that the formation of some metal silicides on the metal surface during a high-temperature catalyst reduction should always be considered.

Romanowski and Lamber (*8*) have found

Address: Institute of Low Temperature and Structure. Research, Polish Academy of Sciences, 50-950 Wrocław, P.O. Box 937, Poland

[1] This work has been carried out at the University of Bremen.

0021-9517/90 $3.00

that after thermal treatment of the Pt/SiO_2 system under high vacuum at 823 K a new phase appears, which has been tentatively ascribed to platinum silicide. This finding was confirmed in experiments carried out in a hydrogen atmosphere, where platinum silicide was identified (*9, 10*) by means of electron diffraction.

The behavior of some silica-supported catalysts with respect to adsorption and catalytic activity seems to be similar to that observed for TiO_2-supported catalysts after high-temperature reduction which was attributed to a strong metal–support interaction (SMSI) (*11, 12*), although the mechanism of this phenomenon could be different for different systems.

The present work was undertaken in order to investigate in more detail the influence of the SiO_2 substrate pretreatment on the metal–support interaction. Experiments were carried out on model Pd/SiO_2 catalysts composed of a thin layer of SiO_2 and vacuum-evaporated palladium, enabling electron microscopic observation.

EXPERIMENTAL

Preparation of SiO_2 Substrates

SiO_2 substrates, as thin (25–30 nm) films, were prepared by oxidation of SiO films. The latter were obtained by sublimination in a vacuum of a piece of SiO onto a fresh, air-cleaved (100) face of a NaCl single crystal. After sublimation the NaCl substrate was immersed in a large amount of distilled water and the floating SiO films were picked up on gold or platinum electron microscope grids. In order to obtain SiO_2, the SiO films were oxidized by heating at 900 K in an air atmosphere for 30 h. Electron diffraction analysis of the SiO_2 substrate showed only the presence of two diffuse rings, indicating that the substrates were amorphous. The EM grids with SiO_2 substrates were mounted in a standard vacuum apparatus with a base pressure of 2×10^{-5} Pa, where deposition of palladium and thermal treatment in a hydrogen atmosphere were carried out.

Deposition of Palladium

Palladium was deposited by vacuum evaporation from a resistance-heated tungsten boat. The metal loading was varied by controlling the amount of evaporated metal. During evaporation the pressure was kept below 2×10^{-4} Pa.

Thermal Treatment

The EM grids were placed in a resistance-heated tantalum holder located in the vacuum bell-jar. The tantalum holder allowed the heating of the EM grids with the SiO_2 supports before and after Pd evaporation. The temperature was measured using a Pt–(Pt–Rh) thermocouple spot-welded directly to the Ta holder. After the Pd layer had been evaporated, hydrogen was supplied to the vacuum cell at a pressure of 6×10^{-2} Pa and a constant flow rate, and the thermal treatment of the Pd/SiO_2 system was carried out.

Electron Microscopy

All specimens were examined in a Philips EM 420 T transmission electron microscope operated at 120 kV and equipped with an energy dispersive X-ray analyzer (EDX). In the EDX spectrum obtained from the Pd/SiO_2 system only the peaks due to Pd, Si, and Au (Au EM grids) were visible. No extra peaks due to impurities could be detected. The microscope was operated with the lowest possible illumination intensity in order to minimize any influence of the radiation.

RESULTS

Growth of Palladium Particles

In order to detect the influence of the state of SiO_2 surface on the growth of metal particles and the metal–support interaction, experiments with different thermal pretreatment of the SiO_2 substrate were carried out. The SiO_2 substrate of specimen A had been heated at a temperature of 850 K in a vacuum for 10 h before the palladium was evaporated. The substrate of specimen

B was heated at 420 K for 1 h. It should be noted that heating of silica at temperatures around 370 K leads to the desorption of physically adsorbed water (specimen B), while thermal treatment at temperatures about 670 K causes desorption of the chemisorbed water, which is present on the silica surface as silanol (SiOH) groups. If the sample is heated above 770 K, relocation of the surface ions occurs and a passive surface results, on which readsorption of water is slow (*13*) (specimen A).

After the SiO_2 substrate had been cooled to 300 K, palladium films about 0.4 nm in thickness were prepared by evaporation. After deposition of the films the vacuum

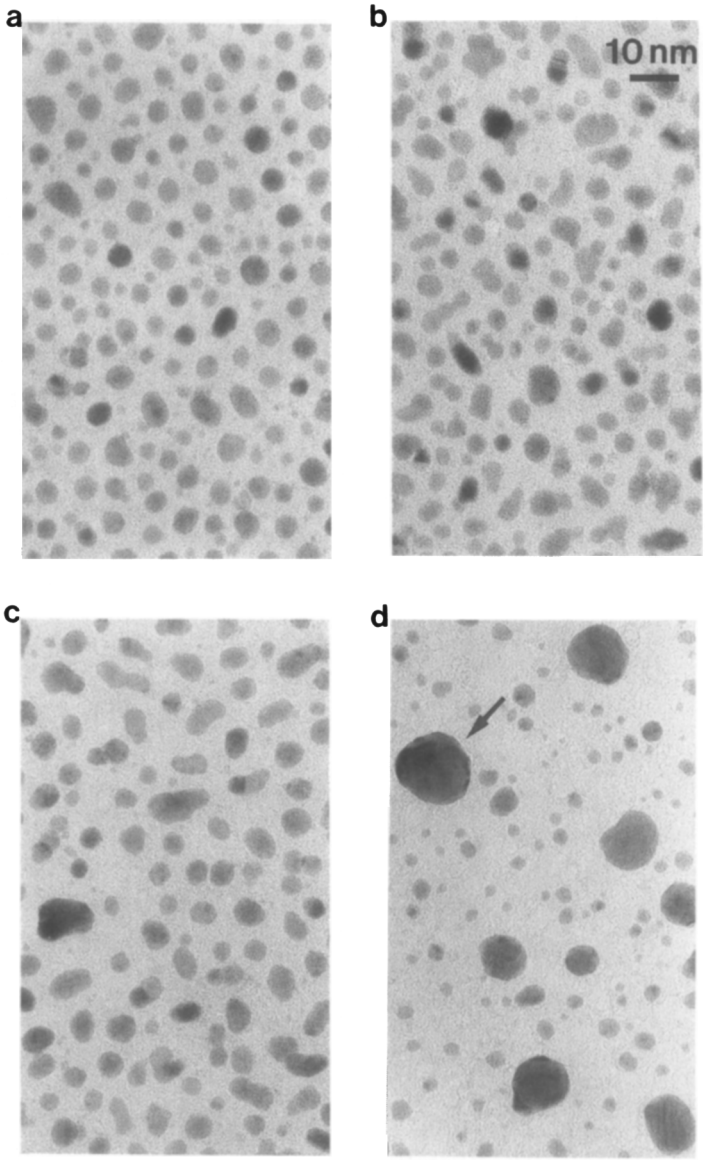

FIG. 1. Electron micrographs of the model Pd/SiO_2 specimen after heating in H_2. (a) Specimen A, 820 K, 10 h; (b) specimen B, 820 K, 10 h; (c) specimen A, additional 845 K, 90 h; (d) specimen B, additional 845 K, 90 h.

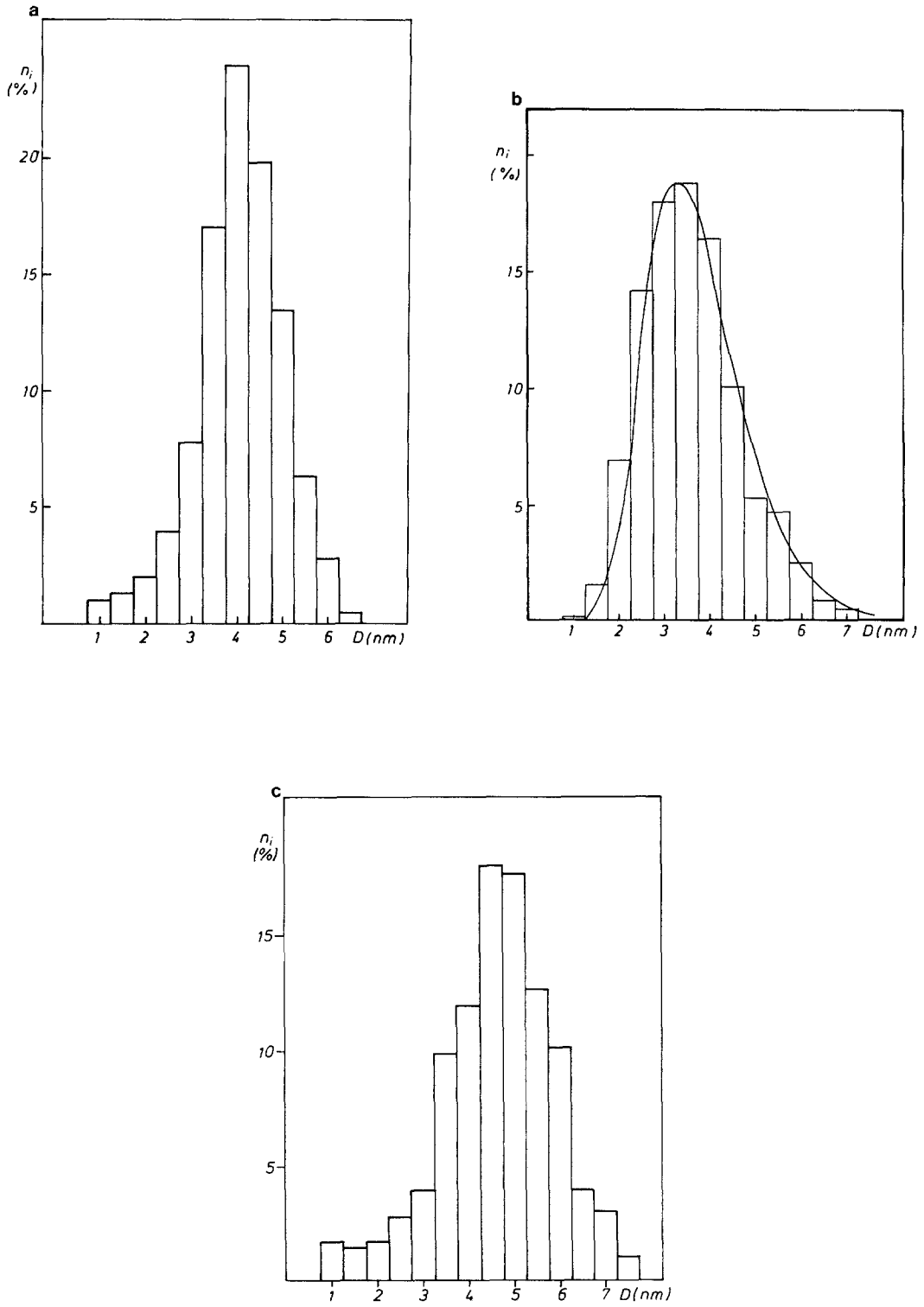

FIG. 2. Particle size histograms for the model Pd/SiO_2 system at the stages a–d of Fig. 1. The fitted curve (histogram b) represents a log-normal size distribution within $\bar{D} = 3.25$ nm, $\sigma = 1.34$.

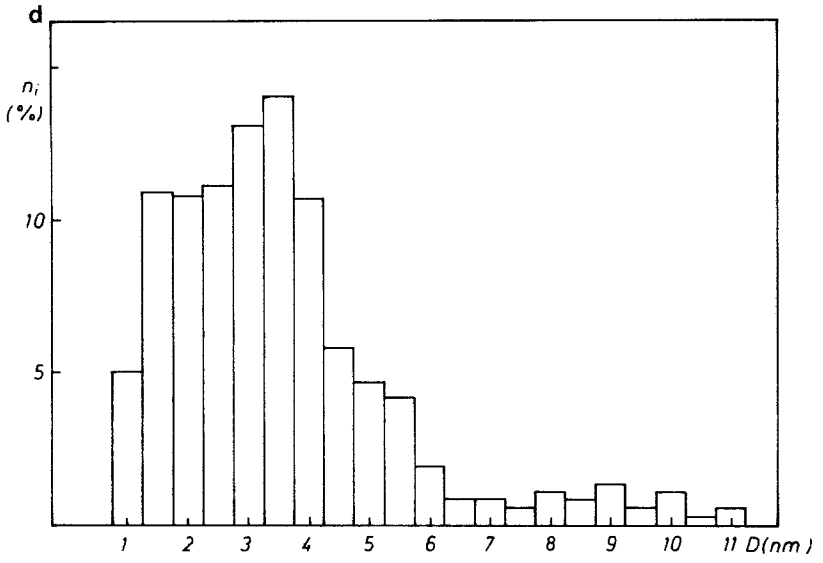

FIG. 2—*Continued*

cell was flushed with hydrogen at the pressure of 6×10^{-2} Pa and the specimens were heated at a rate of 10 K min^{-1} to 820 K and maintained for 10 h at this temperature. Palladium crystallites obtained after this thermal treatment are shown in Figs. 1a (specimen A) and 1b (specimen B). In the case of specimen A (Fig. 1a) most of the particles have a round shape. The average particle size is 4.4 nm and was calculated by the formula

$$\bar{D} = \frac{\sum n_i \cdot \bar{D}_i^3}{\sum n_i \cdot \bar{D}_i^2}$$

where n_i is the number of particles within the diameter D_i; $D_i + \Delta D$, and $\bar{D}_i = D_i + \Delta D/2$. The size histogram shown in Fig. 2a is narrow—i.e., over 80% of particles have diameters in the range 3–5 nm—and has a tail on the small-diameter side. Palladium particles obtained in the case of specimen B (SiO_2 pretreatment at 420 K) are shown in Fig. 1b. The shape of most particles is rather complicated and seems to be caused by interfusion of crystallites with each other. The particle size histogram is shown in Fig. 2b. This size histogram is broader compared to that of sample A, has a tail on the large-diameter side, and agrees well with a log-normal distribution predicted by Granqvist and Buhrman (*14*) for growth by particle migration and coalescence.

The next stage of thermal treatment consisted in heating specimens A and B in hydrogen at 845 K for 90 h. In the case of specimen A this additional heat treatment resulted in some increase in the average particle size to 5.1 nm and an increase in the width of the distribution (Fig. 2c). The electron micrograph of sample B after reduction at 845 K is shown in Fig. 1d. The thermal treatment at 845 K results in distinct changes in the particle morphology (Figs. 1b and 1d) and a considerable number of particles of sizes in the range 7–11 nm appears and can be seen as a large-particle mode on the corresponding size histogram (Fig. 2d): the average size consequently increases to 5.7 nm.

Electron Diffraction

Electron diffraction analysis of specimens after heat treatment at 820 K showed the presence of diffraction rings characteristic for fcc crystallites in random orientations (Fig. 3). A lattice parameter $a_0 = 0.390 \pm 0.004$ nm has been obtained, which

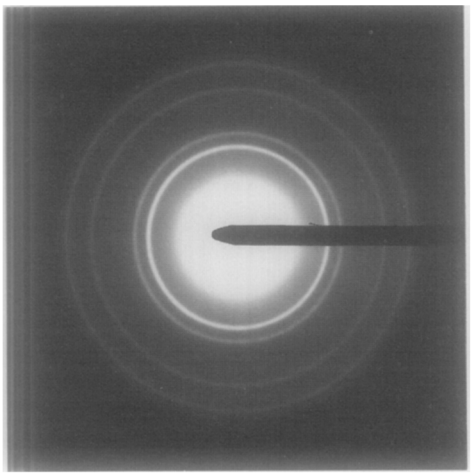

FIG. 3. Selected area electron diffraction pattern obtained for specimen A heated at 820 K, 10 h. The diffraction rings (111), (200), (220), (311) and (222) of the fcc Pd are visible.

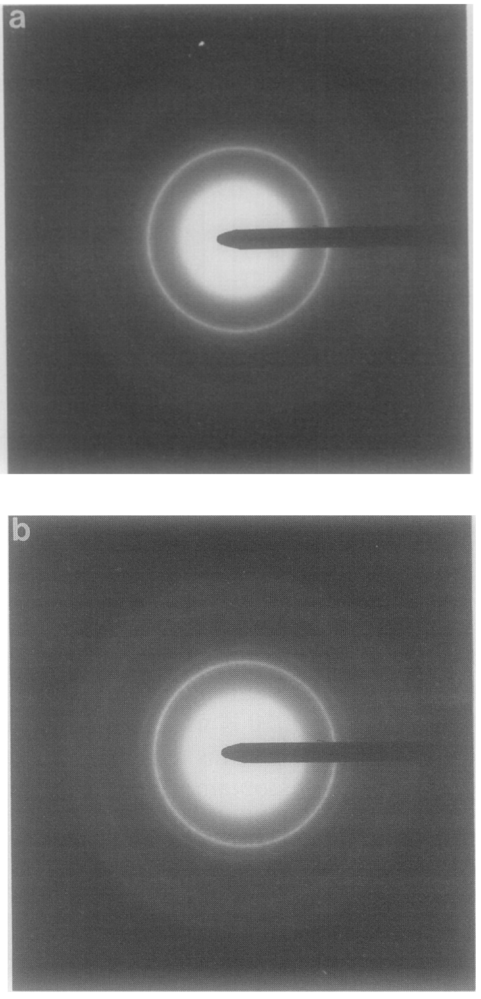

FIG. 4. Selected area diffraction patterns obtained after heating at 845 K, 90 h. (a) Specimen A; (b) specimen B.

corresponds to that of the bulk Pd metal (a_0 = 0.389 nm).

The electron diffractograms of specimens A and B after thermal treatment of 845 K are shown in Figs. 4a and 4b. Careful analysis of these diffractograms revealed that in the vicinity of the (111) ring of fcc phase ($d_{(111)}$ = 0.2246 nm) two additional diffraction rings are visible (Figs. 4a,b). These additional diffraction rings correspond to interplanar spacings d = 0.237 nm and d = 0.211 nm. They cannot be explained by the presence of twinned crystallites or double diffraction effects. The formation of a new Pd–Si phase can be expected after prolonged heat treatment of the Pd/SiO_2 system at 845 K in a hydrogen atmosphere (*2*). The observed lines in the diffractograms are not sufficient to identify any of the known Pd–Si compounds Pd_5Si, Pd_9Si_2, Pd_3Si, and Pd_2Si (*15–17*).

Microdiffraction Analysis

For further characterization of the Pd/SiO_2 system heated at 845 K the method of convergent beam diffraction has been employed. In some cases it was possible to obtain microdiffraction patterns, which allowed the recognition of the new phase and their structural relationship with the basal palladium particles. In Figs. 5–7 three convergent beam diffraction patterns are shown together with the analysis of the diffractograms. These patterns are examples for the superposition of the diffraction patterns due to Pd single crystals and the Pd_2Si phase. Pd_2Si has a hexagonal structure with a = 1.3055 nm and c = 2.749 nm (*16*).

The pattern shown in Fig. 5a can be indexed as the superposition of the diffraction patterns of the Pd crystal in the $[111]_c$

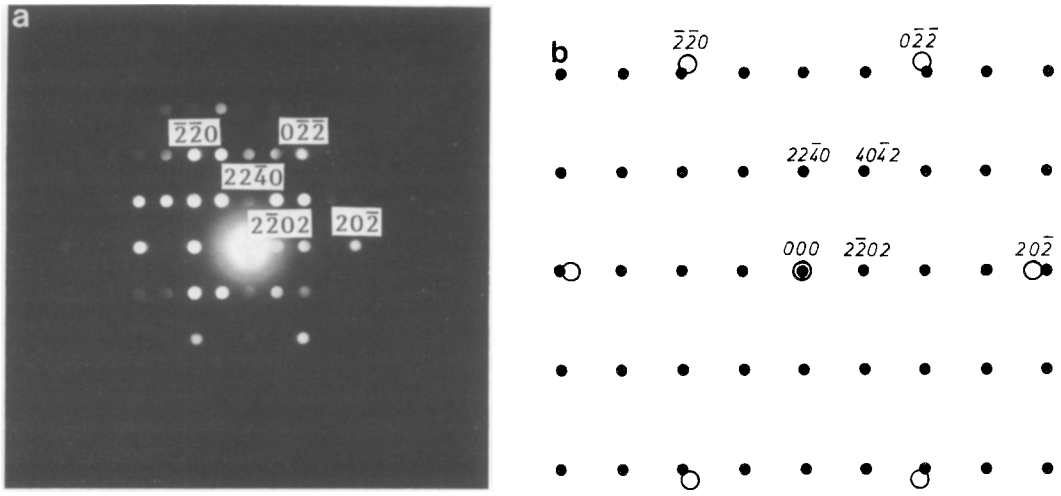

FIG. 5. (a) Microdiffraction pattern, due to Pd single crystal-$[\bar{1}1\bar{1}]_c$ zone and Pd_2Si-$[\bar{1}\bar{1}2]_h$ zone. (b) Interpretation of Fig. 5a: Open spots represent palladium reflections, $[\bar{1}1\bar{1}]_c$ zone; dark spots Pd_2Si reflections, $[\bar{1}\bar{1}2]_h$ zone.

orientation and Pd_2Si in the $[\bar{1}\bar{1}2]_h$ orientation. The subscripts "c" and "h" are used to indicate the cubic and hexagonal phases, respectively. Detailed analysis of Fig. 5a is given in Fig. 5b. An example of another microdiffraction pattern is shown in Fig. 6a. The interpretation of the diffraction pattern is given in Fig. 6b. The spots belong to the Pd $[00\bar{1}]_c$ and the Pd_2Si $[\bar{1}\bar{2}12]_h$ zones.

The diffraction pattern shown in Fig. 7a reveals the presence of the metal fcc phase in the $[\bar{1}\bar{2}\bar{3}]_c$ orientation and Pd_2Si in the $[\bar{1}\bar{2}\bar{6}1]_h$ orientation. Detailed analysis of Fig. 7a is given in Fig. 7b.

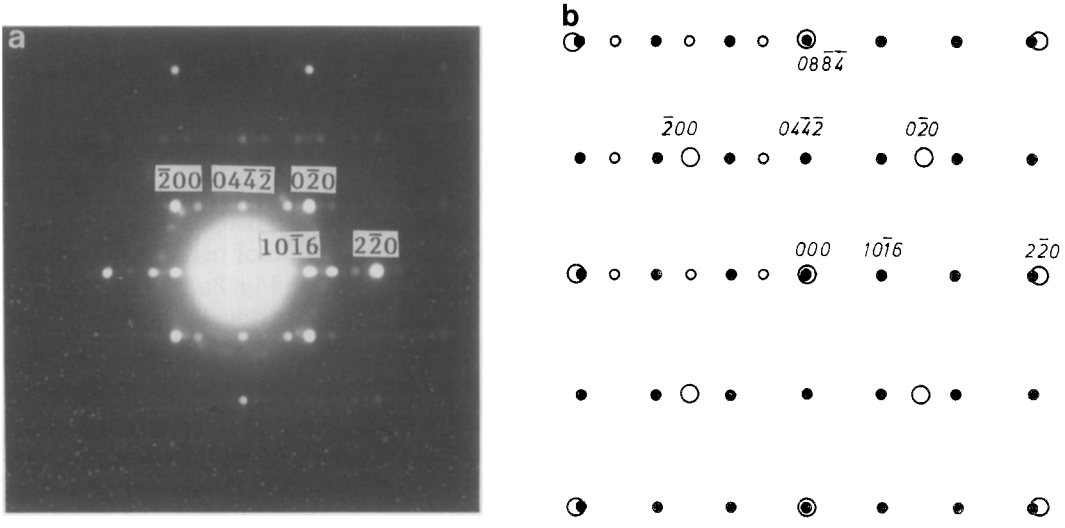

FIG. 6. (a) Microdiffraction pattern due to Pd single crystal in the $[00\bar{1}]_c$ orientation and Pd_2Si in the $[\bar{1}\bar{2}12]_h$ orientation. (b) Interpretation of Fig. 6a: open spots, $[00\bar{1}]_c$ Pd zone; dark spots, $[\bar{1}\bar{2}12]_h$ Pd_2Si zone. Small open spots represent double diffraction spots due to $(\bar{2}00)$ Pd as secondary source.

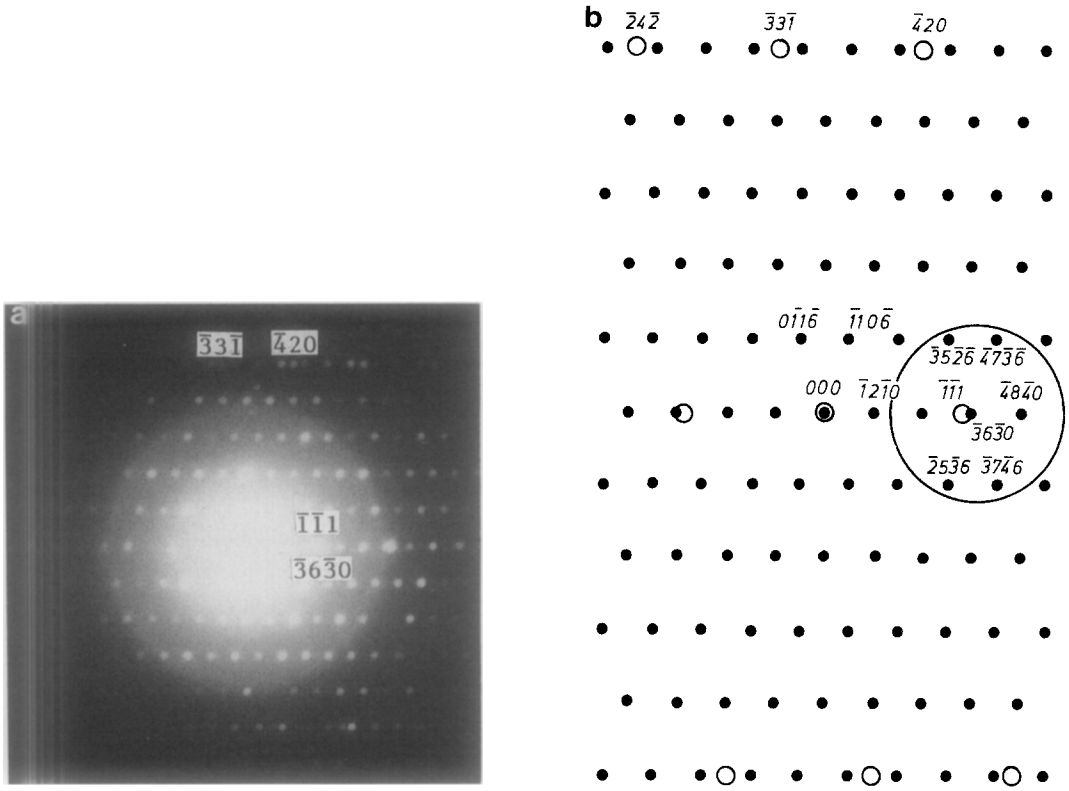

FIG. 7. (a) Microdiffraction pattern due to Pd in the $[\bar{1}2\bar{3}]_c$ orientation and Pd_2Si in the $[\bar{1}2\bar{6}1]_h$ orientation. (b) Interpretation of Fig. 7a: Open spots, $[\bar{1}2\bar{3}]_c$ Pd zone; dark spots, $[\bar{1}2\bar{6}1]_h$ Pd_2Si zone. The encircled diffracted beams were used in obtaining the dark field image shown in Fig. 8a.

High-Resolution Observations

When two crystals with different lattice parameters or orientations overlap, an indirect lattice image (moiré pattern) may be produced. As a result of the overlap of the Pd crystallites with palladium silicide, many particles revealed the presence of moiré fringes. In some cases it was possible to obtain a direct image of Pd_2Si lattice fringes. In Fig. 8a one can see the dark field image of the arrowed particle in Fig. 1d. Microdiffraction analysis of this particle revealed the presence of the Pd_2Si phase in the $[\bar{1}2\bar{6}1]_h$ orientation (see Figs. 7a and 7b). For imaging the diffraction vectors g = $\{\bar{2}5\bar{3}6\}$, $\{\bar{3}7\bar{4}6\}$, $(\bar{2}4\bar{2}0)$, $(\bar{3}6\bar{3}0)$, $(\bar{4}8\bar{4}0)$ of Pd_2Si and g = $(\bar{1}\bar{1}1)$ of Pd were used. Two sets of lattice fringes with spacings of about 0.4 nm and one set of lattice fringes with spacings of about 0.7 nm are visible. The fringes with spacings of 0.4 nm correspond to $\{\bar{1}10\bar{6}\}$ Pd_2Si lattice fringes ($d_{(\bar{1}10\bar{6})}$ = 0.425 nm). The 0.7-nm lattice fringes correspond to $(\bar{1}2\bar{1}0)$ Pd_2Si lattice fringes ($d_{(\bar{1}2\bar{1}0)}$ = 0.653 nm). The observation of bending of the 0.4-nm fringes (arrow in Fig. 8a) seems to indicate the presence of dislocations in the Pd_2Si lattice. In Fig. 8b the bright field image of a particle showing lattice fringes with spacings 0.35 nm is shown. From a microdiffraction pattern obtained from this particle it could be concluded that these are $(20\bar{2}6)$ lattice planes of Pd_2Si ($d_{(20\bar{2}6)}$ = 0.356 nm). It is interesting to note that these fringes are visible ony in part of the particle (Fig. 8b).

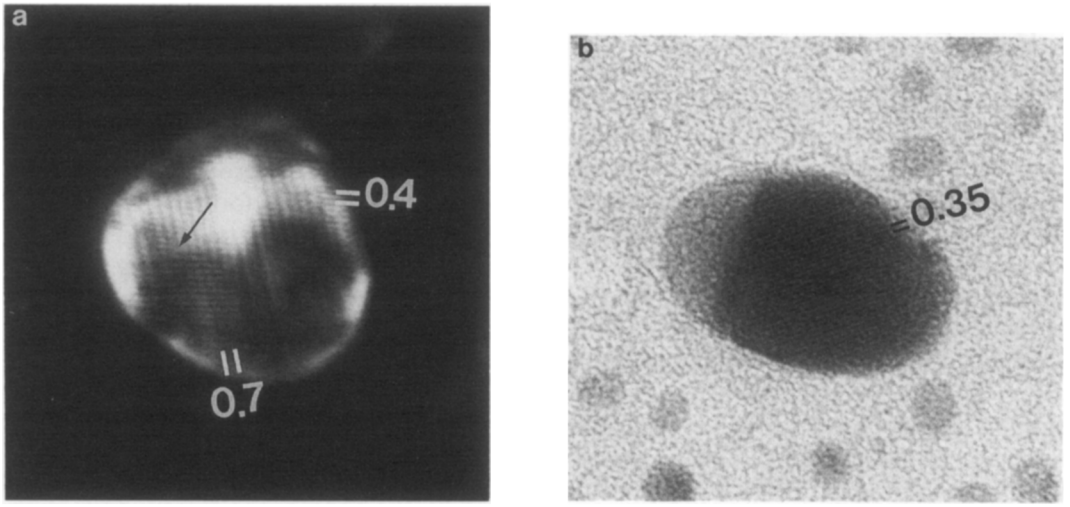

FIG. 8. (a) Dark field image of arrowed particle in Fig. 1d. Two sets of fringes with spacings about 0.4 nm correspond to $\{\bar{1}10\bar{6}\}$ lattice fringes ($d_{(\bar{1}10\bar{6})Pd_2Si}$ = 0.425 nm). Fringes with spacings of about 0.7 nm correspond to $(\bar{1}2\bar{1}0)$ Pd_2Si lattice fringes ($d_{(\bar{1}2\bar{1}0)Pd_2Si}$ = 0.653 nm) (see Fig. 7b). (b) A particle showing 0.35-nm fringes corresponding to $(20\bar{2}6)$ Pd_2Si lattice planes (d = 0.356 nm).

DISCUSSION

Pretreatment of the SiO_2 Substrate and Growth of Pd Particles

Assuming different migrating species on the surface, two different mechanisms have been proposed to explain the size change of metal particles dispersed on the substrate. Growth through the random migration of metal particles across the support surface followed by collision and coalescence have been proposed by Ruckenstein and Pulvermacher (*18, 19*). The other mechanism proposed by Flynn and Wanke (*20, 21*) assumes the migration of metal atoms (or molecular species) from small particles to large ones.

Granqvist and Buhrman (*22*) pointed out that the shape of the histograms can be used as a means to determine the mechanism by which the particles have grown. Size distributions obtained by Wynblatt and Gjostein (*23*) for growth by migration of atoms have two characteristic features: these are a tail on the small diameter side and a sharp cut-off immediately beyond the peak in the distribution. A log-normal distribution, predicted for growth by particle coalescence on the other hand has a tail on the large-diameter side where the distribution approaches zero asymptotically (*14*). The size histogram obtained after the first stage of the heat treatment of sample A (Fig. 2a) corresponds to that predicted for growth by atomic diffusion, and the histogram obtained for sample B (Fig. 2b) is log-normal as predicted for a growth mechanism by particle coalescence. Since the only significant difference between specimens A and B was the state of the substrate surface caused by different thermal pretreatments, we can assume that the growth of palladium particles is strongly influenced by the state of the SiO_2 surface. The presence of the chemisorbed water in the form of SiOH (sample B) seems to favor the migration of particles and growth by their coalescence. The growth of palladium particles on the OH-depleted surface of silica proceeds by atom diffusion (sample A).

Pretreatment of the SiO_2 Substrate and Metal–Support Interaction

The mechanism which actually governs the size change in metal particles is strongly dependent on the magnitude of metal–support interaction. Recently, detailed transmission electron microscopy of metal particles on oxide supports and carbon has been carried out in order to evaluate the strength of the metal–support interaction (*23–28*). It is believed that the atomic migration mechanism is more significant when the metal–support interaction is strong. Stronger interaction of metal atoms with the support facilitates the escape of an atom from the particle, which is considered as the process requiring the largest energy (*20, 21*). In the particle migration mechanism a random thermal motion of the metal atoms plays an important role (*19, 23*). This thermal motion may result in the deformation and subsequent movement of a particle, provided that the particle movement is not suppressed by strong bonds between metal atoms and support. Therefore the particle migration mechanism would predominate when metal–support interaction is weak. From the above consideration it can be concluded that the change in the growth mechanism observed in our experiment and caused by the thermal pretreatment of the SiO_2 substrate should be connected with the change in the magnitude of metal–support interaction or chemistry of metal–support interface. As was noted, heating of silica above 770 K causes desorption of chemisorbed water and leads to the relocation of surface atoms. It seems very probable that by this high-temperature treatment the creation of some oxygen vacancies on the SiO_2 surface takes place. We believe that the existence of the oxygen vacancies may lead to a strong metal–silicon interaction and results in the stabilization of small palladium particles obtained after evaporation. The size change of these strongly bonded metal particles may proceed predominantly through atomic migration. The presence of OH groups on the SiO_2 surface might prevent chemical metal–support interaction and enable particle diffusion in the first heating stage of specimen B. However, during heating of the Pd/SiO_2 system the desorption of OH groups proceeds and the possibility of the formation of metal–silicon bonds should be taken into account. This possibility is supported by the detected formation of the intermetallic compound.

Growth of Palladium Silicide

Direct evidence for strong interaction between palladium and silicon dioxide is provided by the appearance of new diffraction rings in addition to those of palladium in the electron diffraction diagrams. The method of convergent beam diffraction allowed the identification of the Pd_2Si palladium silicide. The formation of palladium silicide under the condition of the present experiments most probably occurs by the reduction of SiO_2 in the presence of palladium:

$$2Pd + SiO_2 + 2H_2 \rightleftharpoons Pd_2Si + 2H_2O. \quad (1)$$

The presence of atomic hydrogen due to the dissociative adsorption of H_2 on Pd renders this reaction energetically attractive. It is also known that hydrogen is dissolved into the bulk of the Pd (*30*), which might facilitate the penetration of the metal–substrate interface by hydrogen.

By careful comparison of the diffraction patterns obtained from samples A and B (Figs. 4a and 4b) some additional information regarding the growth of palladium silicide can be obtained. The Pd_2Si diffraction rings in Fig. 4a are diffuse, indicating a very small Pd_2Si crystallite size. In contrast to sample A, the narrower diffraction rings shown in Fig. 4b (sample B) give evidence of larger Pd_2Si crystallites. We suggest that this difference could be explained by the presence of silanol groups (SiOH) on the surface of sample B. In this case another reaction should be considered:

$$2Pd + SiOH + \tfrac{1}{2}H_2 \rightleftharpoons Pd_2Si + H_2O. \quad (2)$$

We believe that reaction (2) could provide a potential mechanism for the faster growth of palladium silicide.

The characterization of the Pd/SiO_2 system by means of covergent beam diffraction showed the presence of palladium silicide in the case of Pd particles either with dense-packed planes like (111), (100) (Figs. 5a and 5b and 6a and 6b) or with more open planes like (123) (Figs. 7a and 7b) oriented parallel to the substrate. Analysis of the diffraction patterns given in Figs. 5, 6, and 7 shows that some lattice spacings of the Pd_2Si precipitates are integral multiples of those of the Pd matrix. For example: $d_{(\bar{1}2\bar{1}0)Pd_2Si} \approx 3 \cdot d_{(\bar{1}\bar{1}1)Pd}$ (see Figs. 7a and 7b), $d_{(2\bar{2}02)Pd_2Si} \approx 4 \cdot d_{(20\bar{2})Pd}$ (see Figs. 5a and 5b), and $d_{(10\bar{1}6)Pd_2Si} \approx 3 \cdot d_{(2\bar{2}0)Pd}$ (see Figs. 6a and 6b). The lattice misfits $\delta = 2\,(n \cdot d_1 - d_2)/(n \cdot d_1 + d_2)$, $n = 3, 4, 3$, respectively, i.e., the relative differences between the unstrained lattice spacings d_1 (Pd) and d_2 (Pd_2Si) are equal to 12, 5, and -2%, respectively. The fact that the lattice spacings of the Pd_2Si precipitates tend to be integral multiples of those of the Pd matrix can indicate a special or a preferred orientation relationship between the Pd metal and the Pd_2Si phase. From diffraction patterns shown in Figs. 5, 6, and 7 it is possible to determine the orientation relationship, if any, between the two phases. Calculations of the direction cosines of the crystallographic axes of the hexagonal Pd_2Si lattice with respect to the base vectors of the Pd cubic lattice for six different microdiffraction patterns taken in different zone axes lead to the overall mean value

$$[100]_h \parallel [\bar{1}9\ 23\ 95]_c$$
$$[010]_h \parallel [58\ 59\ \bar{5}6]_c$$
$$[001]_h \parallel [\bar{7}9\ 52\ \bar{3}0]_c.$$

The details of the calculation are given in the Appendix.

It can be seen that $[010]_h \parallel [58\ 59\ \bar{5}6]_c$, which is only 1.4° from $[11\bar{1}]_c$. That indicates the parallelism of the $[010]_h$ and $[11\bar{1}]_c$ directions. It is seen that the $[001]_h$ direction is very close (1.4°) to $[\bar{8}5\bar{3}]_c$ or to $[\bar{3}2\bar{1}]_c$ (2.1°). It can be concluded that there is a fixed orientation relationship between the Pd and the Pd_2Si phases: $[010]_h \parallel [11\bar{1}]_c$ and $[001]_h \parallel [\bar{8}5\bar{3}]_c$.

CONCLUSIONS

The present study demonstrates that heating of the Pd/SiO_2 system in a hydrogen atmosphere can lead to strong, chemical interaction between metal and support and growth of palladium silicide Pd_2Si. The microdiffraction study showed a definite orientation relationship between these two phases: $[010]_{Pd_2Si} \parallel [11\bar{1}]_{Pd}$ and $[001]_{Pd_2Si} \parallel [\bar{8}5\bar{3}]_{Pd}$. The metal–support interaction, particle agglomeration, and intermetallic compound formation are strongly influenced by thermal pretreatment of the SiO_2. OH groups on the silica facilitate the particle migration and growth by coalescence, whereas on OH-depleted silica particle size changes proceed by atomic diffusion. On the other hand, silanol groups may facilitate chemical metal–support interaction and the formation of an intermetallic compound. In the presence of chemical interaction between palladium and silica the possibility of the diffusion of the constituent elements of the support onto the metal surface should also be taken into account. This process may result in a modification of the catalytic properties of silica-supported catalysts, as has been shown for TiO_2-supported catalysts (*29, 31–36*).

APPENDIX

In order to see whether there is a special orientation relationship between the Pd and Pd_2Si phases we choose three non-coplanar vectors of each of the two phases contributing to the diffraction pattern of Fig. 5a. We assume that the zone axes of the Pd and the Pd_2Si phases are parallel and measure the angles between the reciprocal lattice vectors in Fig. 5a. The angular relationships given in Table 1 are obtained.

From these data the direction cosines of the crystallographic axes of the hexagonal

TABLE 1

Angular Relationships between Three Noncoplanar Vectors of the Pd abd Pd_2Si contributing to the diffraction pattern of Fig. 5a

	$(20\bar{2})_c$	$(\bar{2}4\bar{2})_c$	$[\bar{1}1\bar{1}]_c$
$(2\bar{2}02)_h$	0°	90°	90°
$(2\bar{2}40)_h$	90°	0°	90°
$[\bar{1}12]_h$	90°	90°	0°

Pd_2Si phase with respect to the base vectors of the cubic Pd phase can be calculated.

$$[100]_h^1 \parallel [55\ \overline{60}\ \overline{58}]_c$$
$$[010]_h^1 \parallel [\overline{96}\ \overline{22}\ 17]_c$$
$$[001]_h^1 \parallel [\overline{26}\ 53\ \overline{80}]_c.$$

When we change the signs of all Miller indices of the diffraction spots of one phase, we obtain a crystallographically distinct result, since one lattice has been rotated through 180° about a direction which is not an axis of even symmetry. The second orientation relationship obtained in this way from Fig. 5a is given by

$$[100]_h^2 \parallel [\overline{17}\ 22\ 96]_c$$
$$[010]_h^2 \parallel [58\ 60\ \overline{55}]_c$$
$$[001]_h^2 \parallel [\overline{80}\ 53\ \overline{26}]_c.$$

A similar analysis of the diffraction pattern shown in Fig. 6a led to the following orientation relationships:

$$[100]_h^1 \parallel [23\ \overline{23}\ 95]_c \qquad [100]_h^2 \parallel [\overline{23}\ 23\ 95]_c$$
$$[010]_h^1 \parallel [\overline{60}\ \overline{60}\ \overline{53}]_c \qquad [010]_h^2 \parallel [60\ 60\ \overline{53}]_c$$
$$[001]_h^1 \parallel [80\ \overline{51}\ \overline{32}]_c \qquad [001]_h^2 \parallel [\overline{80}\ 51\ \overline{32}]_c.$$

Comparison of these orientation relationships with those obtained in the case of the diffractogram of Fig. 5a shows that the orientation relationships denoted by^2 are very similar. That indicates the true orientation relationship between the Pd and Pd_2Si phases. Analysis of the diffraction pattern shown in Fig. 7a led to the following orientation relationships:

$$[100]_h^1 \parallel [65\ 64\ 42]_c \qquad [100]_h^2 \parallel [\overline{19}\ 26\ 95]_c$$
$$[010]_h^2 \parallel [\overline{58}\ \overline{58}\ 58]_c \qquad [010]_h^2 \parallel [58\ 58\ \overline{58}]_c$$
$$[001]_h^2 \parallel [70\ \overline{71}\ \bar{1}]_c \qquad [001]_h^2 \parallel [\overline{81}\ 50\ \overline{31}]_c.$$

One sees that the orientation relationships denoted by^2 are very similar to those given above. The orientation relationship was measured in this way for six different microdiffraction patterns taken in different zone axes. The overall mean value is as follows:

$$[100]_h \parallel [\overline{19}\ 23\ 95]_c$$
$$[010]_h \parallel [58\ 59\ \overline{56}]_c$$
$$[001]_h \parallel [\overline{79}\ 52\ \overline{30}]_c.$$

It is seen that $[010]_h \parallel [58\ 59\ \overline{56}]_c$, which is only 1.4° from $[11\bar{1}]_c$. It can be concluded that within the experimental error, the hexagonal $[010]_h$ direction is parallel to the cubic $[11\bar{1}]_c$ direction. Since the $[001]_h$ is very close to $[\bar{8}5\bar{3}]_c$ ($[\overline{79}\ 52\ \overline{30}]_c$ is only 1.4° from $[\bar{8}5\bar{3}]_c$ and 2.1° from $[\bar{3}2\bar{1}]_c$) the orientation relationship between the Pd matrix and Pd_2Si precipitates can be given as follows: $[010]_h \parallel [11\bar{1}]_c$ and $[001]_h \parallel [\bar{8}5\bar{3}]_c$.

ACKNOWLEDGMENTS

We thank Professor Dr. W. Romanowski and Professor Dr. P. Ryder for helpful discussions and a critical reading of the manuscript. R. L. gratefully acknowledges financial support by the Deutscher Akademischer Austauschdienst and by the University of Bremen.

REFERENCES

1. Wilson, G. R., and Hall, W. K., *J. Catal.* **24,** 306 (1972).
2. Moss, R. L., Pope, D., Davis, B. J., and Edwards, D. H., *J. Catal.* **58,** 206 (1979).
3. Martin, G. A., and Dalmon, J. A., *React. Kinet. Catal. Lett.* **16**(4), 325 (1981).
4. Martin, G. A., Dutartre, R., and Dalmon, J. A., *React. Kinet. Catal. Lett.* **16**(4), 329 (1981).
5. Martin, G. A., and Dalmon, J. A., *J. Catal.* **75,** 233 (1982).
6. Praliaud, H., and Martin, G. A., *J. Catal.* **72,** 394 (1981).
7. van Langeveld, A. D., Nieuwenhuys, B. E., and Ponec, V., *Thin Solid Films* **105,** 9 (1983).
8. Romanowski, W., and Lamber, R., *Thin Solid Films* **127,** 139 (1985).

9. Lamber, R., *Thin Solid Films* **128,** L 29 (1985).
10. Lamber, R., and Romanowski, W., *J. Catal.* **105,** 213 (1987).
11. Tauster, S. J., Fung, S. C., and Garten R. L., *J. Amer. Chem. Soc.* **100,** 170 (1978).
12. Tauster, S. J., and Fung, S. C., *J. Catal.* **55,** 29 (1978).
13. Morrison, S. R., "The Chemical Physics of Surfaces," Chap. 5. Plenum, New York, 1978.
14. Granqvist, C. G., and Buhrman, R. A., *J. Appl. Phys.* **47,** 2000 (1976).
15. Aronson, B., and Nylund, A., *Acta Chem. Scand.* **14,** 1011 (1960).
16. Nylund, A., *Acta Chem. Scand.* **20,** 2381 (1966).
17. Wysocki, J. A., and Duwez, P. E., *Metall. Trans. A* **12,** 1455 (1981).
18. Ruckenstein, E., and Pulvermacher, B., *AIChE J.* **19,** 356 (1973).
19. Ruckenstein, E., and Pulvermacher, B., *J. Catal.* **29,** 224 (1973).
20. Flynn, P. C., and Wanke, S. E., *J. Catal.* **34,** 390 (1974).
21. Flynn, P. C., and Wanke, S. E., *J. Catal.* **34,** 400 (1974).
22. Granqvist, C. G., and Buhrman, R. A., *J. Catal.* **42,** 477 (1976).
23. Wynblatt, P., and Gjostein, N. A., *Prog. Solid State Chem.* **9,** 21 (1975).
24. Baker, R. T. K., Prestridge, E. B., and Garten, R. L., *J. Catal.* **56,** 390 (1979).
25. Baker, R. T. K., Prestridge, E. B., and Garten, R. L., *J. Catal.* **59,** 293 (1979).
26. Arai, M., Ishikawa, T., and Nishiyama, Y., *J. Phys. Chem.* **86,** 577 (1982).
27. Arai, M., Ishikawa, T., Nakayama, T., and Nishiyama, Y., *J. Colloid Interface Sci.* **97,** 254 (1984).
28. Arai, M., and Nishiyama, Y., *J. Colloid Interface Sci.* **104,** 175 (1985).
29. Singh, A. K., Pande, N. K., and Bell, A. T., *J. Catal.* **94,** 422 (1985).
30. Lewis, F. A., "The Palladium–Hydrogen System." Academic Press, New York, 1967.
31. Mériaudeau, P., Dutel, J. F., Dufaux M., and Naccache, C., *Stud. Surf. Sci. Catal.* **11,** 95 (1982).
32. Santos, J., Phillips, J., and Dumesic, J. A., *J. Catal.* **81,** 147 (1983).
33. Simoens, A. J., Baker, R. T. K., Dwyer, F. J., Lund, C. R. F., and Madon, R. J., *J. Catal.* **86,** 359 (1984).
34. Vannice, M. A., and Sudhaker, C., *J. Phys. Chem.* **88,** 2429 (1984).
35. Ko, C. S., and Gorte, R. J., *J. Catal.* **90,** 59 (1984).
36. Dumesic, J. A., Stevenson, S. A., Sherwood, R. D., and Baker, R. T. K., *J. Catal.* **99,** 79 (1986).